Variations of Undamped Rotor Blade Frequencies Subjected to Transient Heat Flux

Anand M. Sharan* and Rajeeve Bahree†
Memorial University, St. John's, Newfoundland, Canada

In the present work, the variation of rotor blade natural frequencies due to the radiative heat flux has been studied. The dynamic equations of motion have been obtained using curved, 20 node, solid, isoparametric finite elements. The effect of the variation of the pretwist angle on the natural frequencies also has been studied.

Nomenclature

$[A]$ = conduction matrix
$[B]$ = strain-displacement matrix
c = specific heat
$[C]$ = damping matrix
$[CP]$ = capacitance matrix
$[\bar{C}]$ = reduced damping matrix
$[D]$ = material property matrix
e = elemental
$\{F\}$ = dynamic force vector
$\{F_C\}$ = force vector due to convection
$\{F_R\}$ = force vector due to radiation
$\{\bar{F}\}$ = reduced dynamic force vector
g = Gauss point
G = global
h = convective heat transfer coefficient
$[J]$ = Jacobian matrix
K_x = thermal conductivity in the x direction
K_y = thermal conductivity in the y direction
K_z = thermal conductivity in the z direction
$[\bar{K}]$ = reduced stiffness matrix
$[K]$ = stiffness matrix
ℓ_x, ℓ_y, ℓ_z = direction cosines normal to the surface
$[M]$ = consistent mass matrix
$[\bar{M}]$ = reduced mass matrix
n = number of elements
NG = number of Gauss points
$[N]$ = shape function matrix
q = specified heat flux
Q = heat generated within the body
S = surface subjected to convection, radiation, and specified heat flux
t = time
T_∞ = gas temperature
$\{T\}$ = nodal temperature vector
$\{U\}$ = nodal displacement vector
V = volume of the blade
W_i, W_j, W_k = weights used in Gaussian quadrature
Δt = time increment
ϵ = emissivity of the body
θ = angle of pretwist
θ_R = angle of pretwist at root
θ_T = angle of pretwist at tip
ξ, η, ζ = local coordinate directions
ρ = mass density of the material
σ = Stefan-Boltzman constant
χ = a functional
$[\phi]$ = transformation matrix

Received July 13, 1987; revision received April 20, 1988.

*Associate Professor, Faculty of Engineering.
†Graduate Student, Faculty of Engineering.

Introduction

THE free vibration study of the rotor blades is quite important when analyzing dynamic stresses. It is well known that the design of the rotor blades should be carried out in such a way that the forcing frequencies are away from the natural frequencies. But there is a difficulty in carrying out such a design process because the natural frequencies themselves vary during startup of the gas turbine engine. During this stage, the temperature of the blade increases at a rapid rate, thus affecting the stiffness parameters of the system.

The free vibration study of the rotor blades has been carried by various researchers. Subrahmanyam and Leissa[1] and Hutchinson and Zillmer[2] modeled the blade as having a rectangular cross section and carried out the vibration analysis in terms of the bending modes. The influence of taper when using finite-element methods was studied by Banerji and Williams[3] and Gupta.[4] Sisto and Chang[5] used finite-element methods to calculate the natural frequencies; however, their modeling was appropriate only for thin, high-aspect-ratio blades.

As mentioned earlier, the effect of the variation of temperature on the natural frequencies is quite important and is the focus of the present work. In order to accurately model the dynamics of the blade, curved, solid, C° continuity, "serendipity," 20 node isoparametric finite elements have been used; C° continuity implies that the field variables (displacements) here are continuous across the faces of the element. By modeling in this way, the asymmetry, pretwist, and taper of the three-dimensional geometry of the turbine blade can be taken into consideration. Since the size of the global matrices are very large when one uses finite elements, a dynamic matrix reduction scheme has also been used in the present investigation.

Mathematical Formulation

Transient Temperature Analysis

The governing partial differential equation for heat conduction in solids is

$$K_x \frac{\partial^2 T}{\partial x^2} + K_y \frac{\partial^2 T}{\partial y^2} + K_z \frac{\partial^2 T}{\partial z^2} + Q = \rho c \frac{\partial T}{\partial t} \tag{1}$$

with the boundary condition

$$K_x \frac{\partial T}{\partial x} \ell_x + K_y \frac{\partial T}{\partial y} \ell_y + K_z \frac{\partial T}{\partial z} \ell_z + q + h(T - T_\infty) + \sigma\epsilon(T^4 - T_\infty^4) = 0 \tag{2}$$

on the pressure and suction surfaces of the turbine airfoil cross section. Since the hot gases completely enclose the blade, the view factor has been assumed to be equal to 1. Such an assumption is used in any standard textbook.

The equivalent functional formulation of Eq. (1) and its boundary condition [Eq. (2)] can be written in the form shown by Reddy and Sharan[6] as

$$\chi = \int_V \frac{1}{2}\left[K_x\left(\frac{\partial T}{\partial x}\right)^2 + K_y\left(\frac{\partial T}{\partial y}\right)^2 + K_x\left(\frac{\partial T}{\partial z}\right)^2 + 2\,\rho c T\frac{\partial T}{\partial t}\right] dV + \int_S \left[qT + \frac{h}{2}(T - T_\infty)^2 + \sigma\epsilon\left(\frac{T^5}{5} - T_\infty^4 T\right)\right] dS \tag{3}$$

where V is the volume of the turbine blade and S the surface area.

The functional χ can be minimized by equating its first derivative with respect to vector $\{T\}$ to zero. Hence,

$$\sum_{e=1}^{n} \frac{\partial \chi^e}{\partial \{T\}} = 0 \tag{4}$$

Equation (4) can be rewritten in terms of the global matrices using finite-element analysis as

$$[CP^G]\frac{\partial \{T^G\}}{\partial t} + [A^G]\{T^G\} = \{F_C^G\} - \{F_R^G\} \tag{5}$$

where $\{F_R^G\}$ is the global force vector due to radiative heat transfer and contains terms of higher powers of the nodal temperatures. These higher powers of the nodal temperatures make Eq. (5) nonlinear. The details of the global force vector due to radiative heat transfer can be found in the Appendix A. This nonlinear system of equations is solved in the time domain using the Crank-Nicholson finite-difference scheme, which is unconditionally stable.

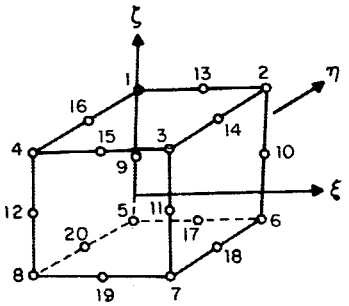

a) Local coordinate system

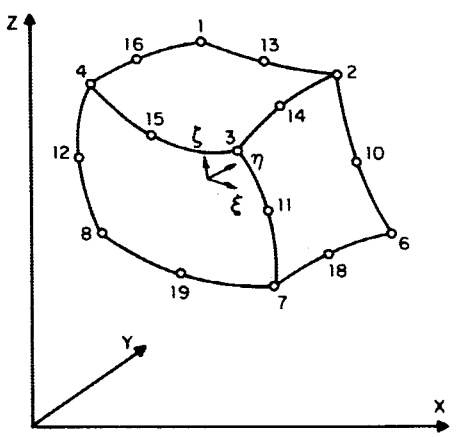

b) Global Cartesian coordinate system

Fig. 1 Solid, isoparametric, "serendipity" 20 node element.

Thus, Eq. (5) can be rewritten as

$$\left[[A^G] + \frac{2}{\Delta t}[CP^G]\right]\{T^G\}_{t+\Delta t} = \left[\frac{2}{\Delta t}[CP^G] - [A^G]\right]\{T^G\}_t + \{F_C^G\}_{t+\Delta t} + \{F_C^G\}_t + \{F_r^G\}_{t+\Delta t} + \{F_r^G\}_t \tag{6}$$

This equation can be solved for the nodal temperature vector $\{T^G\}_{t+\Delta t}$ at every time instant using the iteration procedure mentioned earlier.

At this stage, it should be made clear that the heat-transfer problem has been modeled as a two-dimensional heat flow problem. This is because it can be safely assumed, according to Allen,[7] Mukherjee,[8] and Maya et al.,[9] that for high-aspect-ratio blades there is no significant temperature gradient along the height of the blade. Hence, the term $\partial T/\partial z$ in the Eq. (2) is equal to zero.

Dynamic Analysis of Turbine Blade

In order to model the turbine blade for dynamic analysis, three-dimensional solid finite elements are used. The 20 node, C° continuity, curved, "serendipity" isoparametric element can be chosen for its versatility in accurately mapping the complex geometry of the turbine blade (see Fig. 1). The advantage of isoparametric elements is that the interpolation functions used to describe the geometry of the element and its displacement field are the same. The interpolation functions for this "quadratic" 20 node element can be found in Appendix B and were obtained from Zienkiewicz.[10]

The first task in carrying out the finite-element analysis is to find out the element stiffness matrix $[K^e]$. Mathematically, $[K^e]$ is expressed as

$$\underset{60\times 60}{[K^e]} = \int_V \underset{6\times 6}{[B(x,y,z)]^T}\,\underset{6\times 6}{[D]}\,\underset{6\times 60}{[B(x,y,z)]}\,dx\,dy\,dz = \int_{-1}^{+1}\int_{-1}^{+1}\int_{-1}^{+1} [B(\xi,\eta,\zeta)]^T[D][B(\xi,\eta,\zeta)]|J(\xi,\eta,\zeta)|\,d\xi\,d\eta\,d\zeta \tag{7}$$

The $[K^e]$ matrix for isoparametric elements is evaluated using the second equality. The expression for the $[B]$ matrix in local coordinate system is given by

$$\underset{6\times 60}{[B]} = \underset{6\times 9}{[P]}\;\underset{9\times 9}{[Q]}\;\underset{9\times 60}{[R]} \tag{8}$$

The details of the matrices $[P]$, $[Q]$, and $[R]$ can be found in Appendix B.

Similarly, one can write the expression for elemental mass matrix as

$$[M^e] = \int_V [N]^T\,\zeta[N]\,dx\,dy\,dz = \int_{-1}^{+1}\int_{-1}^{+1}\int_{-1}^{+1} [N(\xi,\eta,\zeta)]^T\rho[N(\xi,\eta,\zeta)]|J(\xi,\eta,\zeta)|\,d\xi\,d\eta\,d\zeta \tag{9}$$

The Jacobian matrix $[J]$ will be

$$[J] = \begin{bmatrix} \frac{\partial x}{\partial \xi} & \frac{\partial y}{\partial \xi} & \frac{\partial z}{\partial \xi} \\ \frac{\partial x}{\partial \eta} & \frac{\partial y}{\partial \eta} & \frac{\partial z}{\partial \eta} \\ \frac{\partial x}{\partial \zeta} & \frac{\partial y}{\partial \zeta} & \frac{\partial z}{\partial \zeta} \end{bmatrix} \tag{10}$$

The element J_{11} of $[J]$ can be written as

$$J_{11} = \frac{\partial x}{\partial \xi} = \underset{1\times 20}{\frac{\partial}{\partial \xi}([N_i]^e)} \underset{20\times 1}{\{x\}^e} \tag{11}$$

where the vector $\{x\}^e$ contains Cartesian coordinates of the 20 node element along the x direction. One can similarly evaluate other elements of the matrix $[J]$.

The final expressions for the matrices $[K^e]$ and $[M^e]$ can be written using a Gaussian quadrature described by Huebner and Thornton[11] as

$$[K^e] = \sum_{i=1}^{NG}\sum_{j=1}^{NG}\sum_{k=1}^{NG} \times W_iW_jW_k\,[B(\xi,\eta,\zeta)]^T\,[D][B(\xi,\eta,\zeta)]\,|J(\xi,\eta,\zeta)| \tag{12}$$

and

$$[M^e] = \sum_{i=1}^{NG}\sum_{j=1}^{NG}\sum_{k=1}^{NG} \times W_iW_jW_k\rho\,\underset{60\times 3}{[N(\xi,\eta,\zeta)]^T}\,\underset{3\times 60}{[N(\xi,\eta,\zeta)]}\,|J(\xi,\eta,\zeta)| \tag{13}$$

The details of the matrix $[N(\xi,\eta,\zeta)]$ are given in Appendix B.

These elemental matrices $[K^e]$ and $[M^e]$ are assembled into global matrices, and the dynamic equation of motion is written as

$$[M^G]\{\ddot{U}\} + [C^G]\{\dot{U}\} + [K^G]\{U\} = \{F(t)^G\} \tag{14}$$

The natural frequencies of the undamped turbine blade can be obtained by solving the eigenvalue problem.

Since matrices $[K^G]$ and $[M^G]$ for this three-dimensional problem become very large, it is quite desirable that a coordinate reduction scheme be used to reduce the size of these matrices without any significant loss of accuracy in terms of the lower modes. One of these schemes is the Guyan's reduction technique.[12]

Dynamic Matrix Reduction

In this dynamic matrix reduction scheme, one makes use of the ratios of the diagonal terms of the stiffness and mass matrices by rearranging these in terms of the ratios K_{ii}/M_{ii}. In this technique, certain degrees of freedom—called slaves—are discarded. The degrees of freedom retained in the reduced matrices are called the masters. The degree of freedom having the largest K_{ii}/M_{ii} ratio is selected as the first slave. In this way, one can rearrange the inertia and stiffness matrices depending upon the number of masters and write the dynamic equation of motion in the form

$$\left[\begin{array}{c|c}[M_{mm}] & [M_{ms}]\\ \hline [M_{ms}]^T & [M_{ss}]\end{array}\right]^G \begin{bmatrix}\ddot{U}_m(t)\\ \ddot{U}_d(t)\end{bmatrix} + \left[\begin{array}{c|c}[C_{mm}] & [C_{ms}]\\ \hline [C_{ms}]^T & [C_{ss}]\end{array}\right]^G \begin{bmatrix}\dot{U}_m(t)\\ \dot{U}_s(t)\end{bmatrix}$$

$$+ \left[\begin{array}{c|c}[K_{mm}] & [K_{ms}]\\ \hline [K_{ms}]^T & [K_{ss}]\end{array}\right]^G \begin{bmatrix}U_m(t)\\ U_s(t)\end{bmatrix} = \begin{bmatrix}F_m(t)\\ F_s(t)\end{bmatrix}^G \tag{15}$$

The reduced system matrices are obtained using the following equations:

$$[\bar{M}^G]_{m\times m} = [\phi]^T_{m\times n}\;[M^G]_{n\times n}\;[\phi]_{n\times m} \tag{16}$$

$$[\bar{K}^G]_{m\times m} = [\phi]^T_{m\times n}\;[M^G]_{n\times n}\;[\phi]_{n\times m} \tag{17}$$

$$[\bar{C}^G]_{m\times m} = [\phi]^T_{m\times n}\;[M^G]_{n\times n}\;[\phi]_{n\times m} \tag{18}$$

$$\{\bar{F}^G\}_{m\times 1} = [\phi]^T_{m\times n}\;\{F(t)^G\}$$

where the transformation matrix $[\phi]$ is given as

$$[\phi] = \begin{bmatrix}[I]\\ \hline -[K_{ss}]^{-1}\,[K_{ms}]^T\end{bmatrix} \tag{19}$$

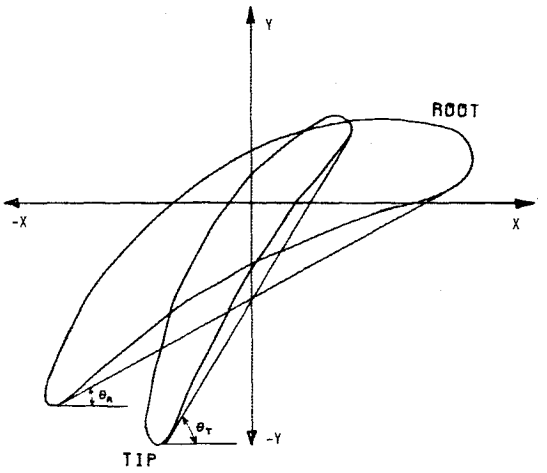

Fig. 2 Blade airfoil cross sections at the root and tip.

Table 1 Geometric and material properties of the blade ($E = 2.1 \times 10^{11}$ Pa, $\rho = 8526$ kg/m^3)

Section	Distance from root $\times 10^2$, m	A $\times 10^4$, m^2	I_{xx} $\times 10^8$, m^4	I_{yy} $\times 10^8$, m^4	θ, deg
1	0.0	2.127	0.3447	0.9489	0.0
2	2.5	1.738	0.3651	0.6717	10.2
3	5.0	1.647	0.4927	0.5174	21.6
4	7.5	1.263	0.5054	0.3097	33.8
5	10.0	1.008	0.4356	0.1543	38.2
6	11.0	0.736	0.3258	0.0858	42.0

Numerical Example

Figure 2 shows two sections of the turbine blade, one at the root and the other at the tip. The height of the blade selected was 0.11 m. This figure also shows the pressure and the suction surfaces where the heat-transfer coefficient h varies along the periphery of the blade. The values of this heat-transfer coefficient were obtained from Mukherjee.[8] The material of the blade was MAR-M200, a superalloy of nickel. The properties of that material, given as a function of temperature, were obtained from Cubberly.[13] It should be added here that the material properties vary with temperature as this blade is heated, a fact included in the present investigation. The angle of twist of this blade can be obtained as the difference between θ_T and θ_R shown in Fig. 2.

For the thermal analysis, it already has been mentioned that one can assume no heat flow in the z direction. Therefore, the two-dimensional thermal analysis is adequate for the present investigation. The discretization of the airfoil section into finite elements is shown in Fig. 3. There were a total of 174 triangular elements, and these were finer near the surface to take into account the steep thermal gradients.

For the dynamic analysis, three-dimensional, 20 node curved isoparametric elements were used. A total of 35 elements were used to describe the blade, with 7 elements across the cross section and 5 layers along the height. There were 308 nodes; therefore, 924 degrees of freedom represent the dynamics of the system. The characteristic details of the blade were obtained from Rao and Yyas[14] are listed in Table 1.

Results and Discussion

Transient Temperature Distribution in Turbine Blade

The transient thermal analysis of the turbine blade was carried out with and without the radiative boundary conditions as given in Eq. (2). In this way, one can clearly see the nonlinearity introduced by the radiative term in the results shown in Fig. 4. In this figure, the trailing edge (point C in

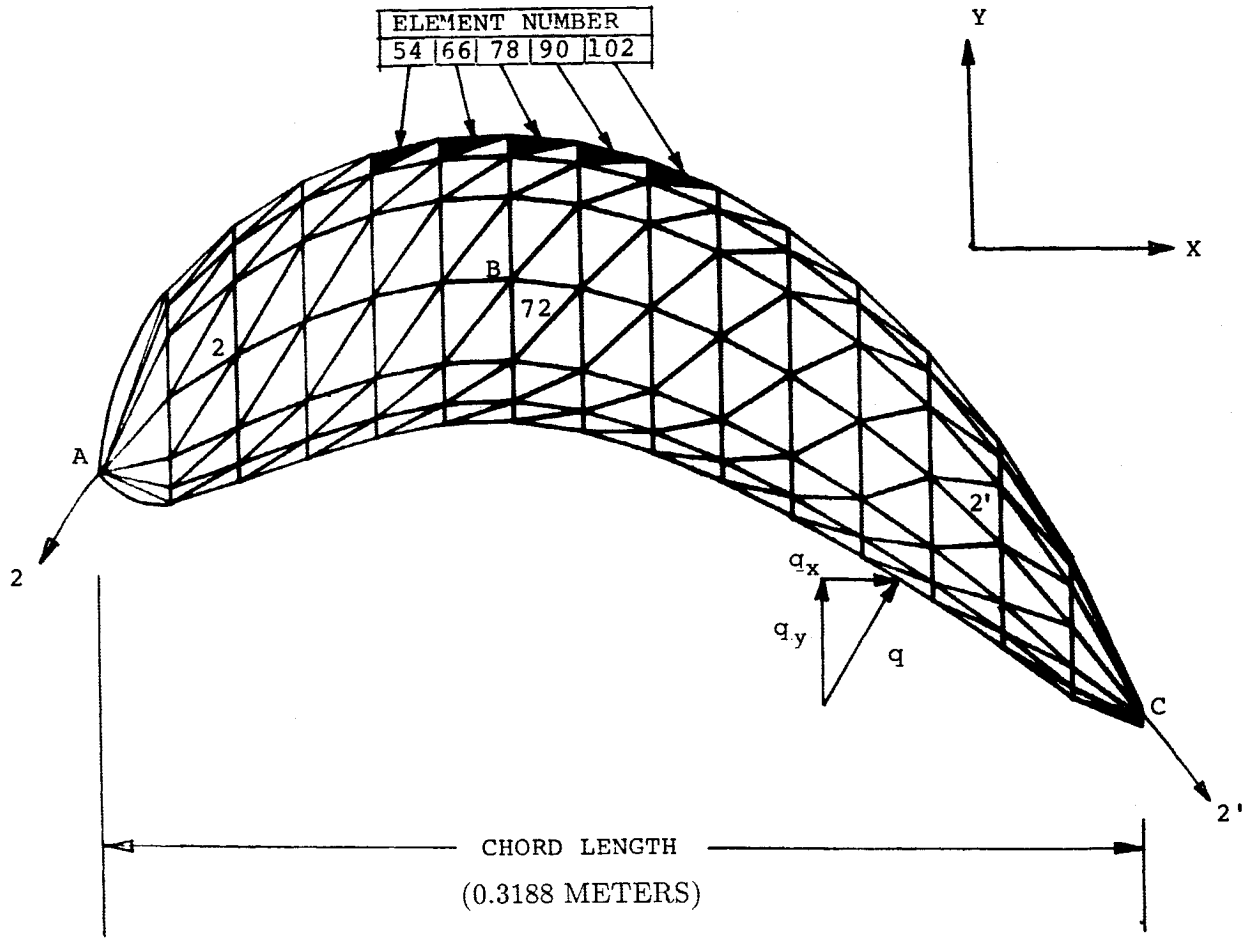

Fig. 3 Finite-element discretization of the turbine blade cross section.

Fig. 3) is always at the highest temperature in the body at any instant of time. It is quite obvious that radiation plays a very important role in the transient thermal analysis of the blade. The temperature of all the three points in Fig. 4 with radiation are significantly higher than those without radiation.

Figure 5 shows the temperature contours at $t = 88$ s across the airfoil cross section. Here one can see that the modulus of elasticity, which plays a significant role in the dynamic analysis, varies from point to point across the airfoil cross section.

Variation of Undamped Natural Frequencies with Temperature

The natural frequencies were obtained by solving the homogeneous part of Eq. (14). As the temperature of the turbine blade changed with time, the stiffness matrix changed, resulting in a variation of the natural frequencies. The results obtained during the heating process at various instants of time are shown in the Table 2, which lists the first 11 natural frequencies. At $t = 1$ s, there is not significant change in the material temperature; therefore, the frequencies in the first column are at ordinary temperatures. But as the material is heated, each of these frequencies starts decreasing due to the decrease in the value of modulus of elasticity. Clearly, there is a very significant change in the natural frequencies in the transient phase. This fact must be included in the design of the turbomachinery. Once the blade has reached the steady-state temperature, these frequencies do not change further. In summary, to calculate these natural frequencies, one has to take into account two types of nonlinearities in the analysis: the first due to the nonlinear radiative boundary conditions and the second due to the nonlinear variations of the material properties of the blade.

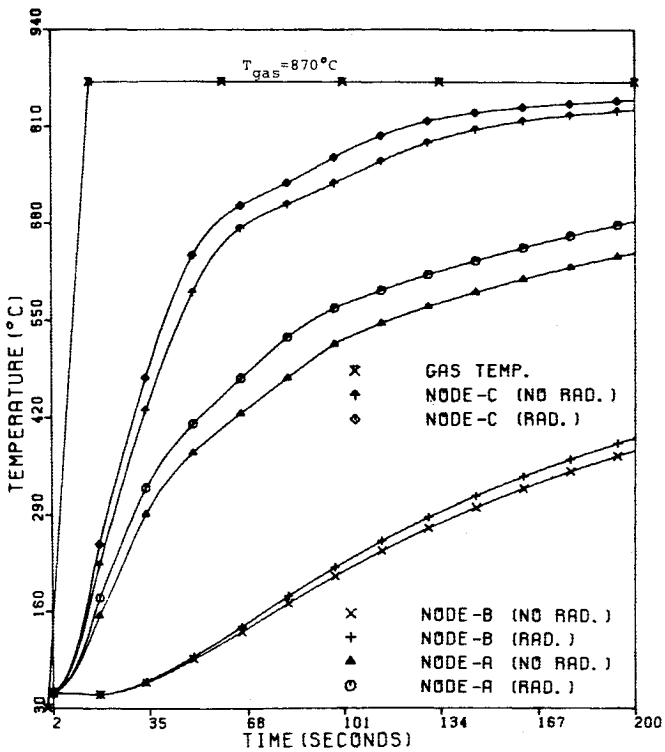

Fig. 4 Transient temperature distribution with and without radiation.

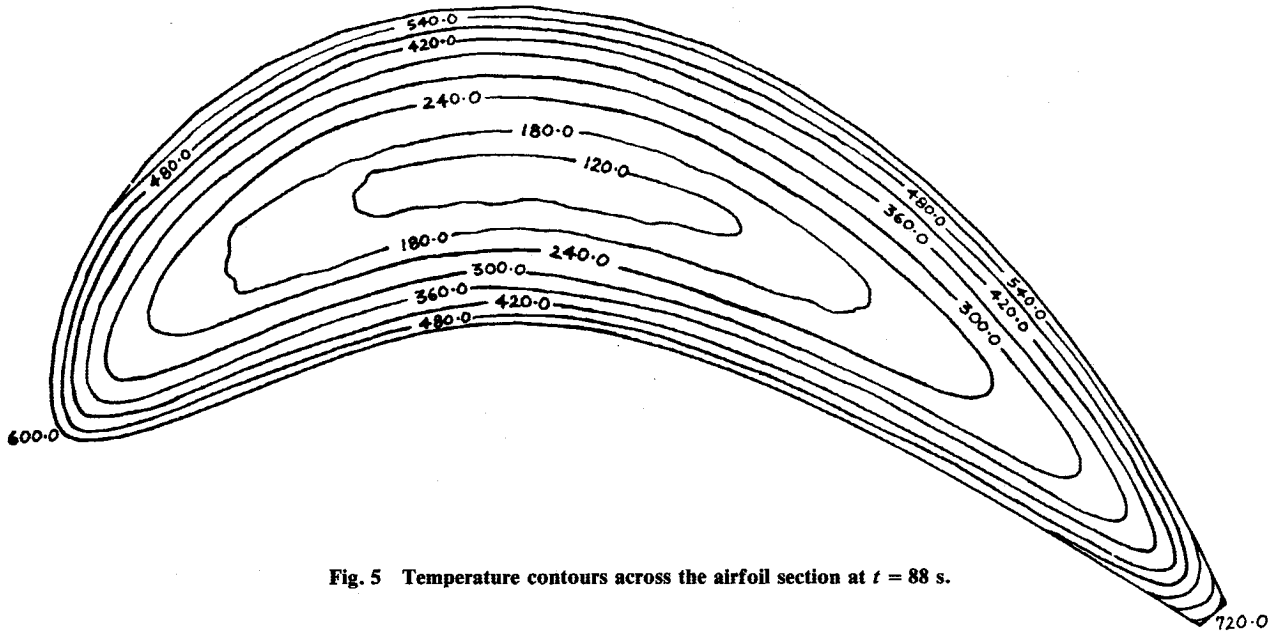

Fig. 5 Temperature contours across the airfoil section at $t = 88$ s.

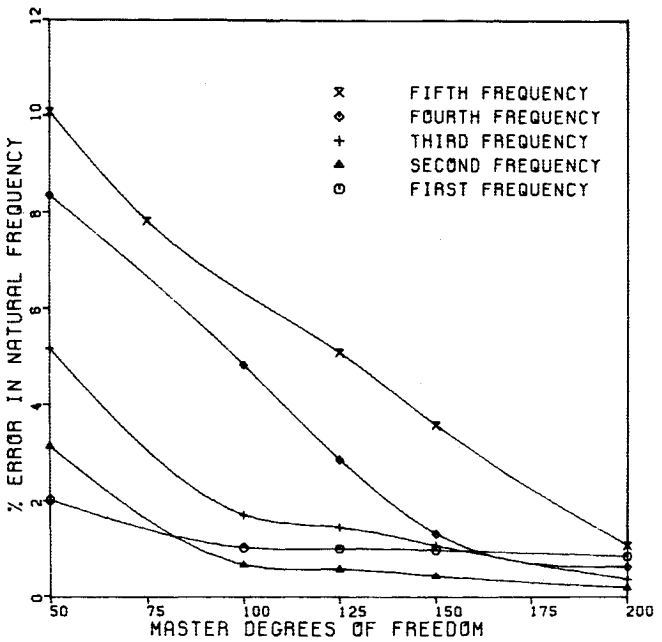

Fig. 6 Plot showing the effect of Guyan's reduction on the first five blade natural frequencies.

Table 2 Variation of natural frequencies (Hz) with time

	Natural frequencies after					
Mode	1 s	30 s	50 s	100 s	120 s	Steady state
I	661.08	651.74	648.48	613.65	603.35	564.58
II	2081.02	2047.43	2001.58	1929.53	1912.24	1784.95
III	3371.59	3310.57	3230.26	3116.24	3094.99	2888.35
IV	4230.02	4171.99	4077.06	3928.37	3900.07	3623.50
V	7159.01	7040.37	6865.78	6629.0	6588.2	6134.51
VI	8891.83	8762.97	8592.89	8261.54	8205.29	7618.53
VII	10956.95	10731.32	10486.71	10118.61	10054.18	9385.74
VIII	13301.75	13118.97	12829.29	12359.61	12280.01	11395.4
IX	15014.76	14777.74	14488.46	13942.27	13848.89	12861.76
X	14232.5	14011.57	13695.39	13198.16	13118.21	12192.42
XI	21803.25	21463.58	21048.37	20259.3	20122.5	18680.02

Suppose for a certain material, the determinant $|A^G| \gg 1$, i.e., the material has very high thermal conductivity but all other properties are the same as for the material used in the present work. In that case, its thermal diffusivity will be very high and all the natural frequencies will change very quickly and approach the steady-state value.

Coordinate Reduction Using Dynamic Matrix Reduction Scheme

As discussed earlier, it almost becomes necessary to reduce the size of the stiffness and mass matrices if one used finite-element analyses. In order to establish the reduced size to these matrices, the error in the first five undamped natural frequencies was used as the selection criteria. Figure 6 shows the percentage error vs the number of master degrees of freedom. From this figure, one can see that as the number of master degrees of freedom is increased, the errors reduce for all the modes. The higher the modes, the greater is the rate of convergence. The error is less than 1% for all the five modes if 200 master degrees of freedom are selected. Therefore, the reduced system containing 200 master degrees of freedom would be adequate to represent the uncondensed system. The presence of large number of master degrees of freedom can be attributed to the asymmetric and twisted geometry of the blade.

Effect of Pretwist on Undamped Natural Frequencies

It is well known that the pretwist angle has a very significant influence on the natural frequencies of the turbine blade. Therefore, the amount of pretwist was varied, and the corresponding natural frequencies obtained. Figure 7 shows the variation of the various modes due to the change in the amount of pretwist. In this figure, all of the bending modes decrease as the pretwist angle is increased. The rate of decrease of these modes per degree change in the twist angle is greater for the higher modes. The torsional modes show just the opposite behavior, i.e., the frequencies increase with the increase in the angle of pretwist. Similar results were obtained by other researchers.[5]

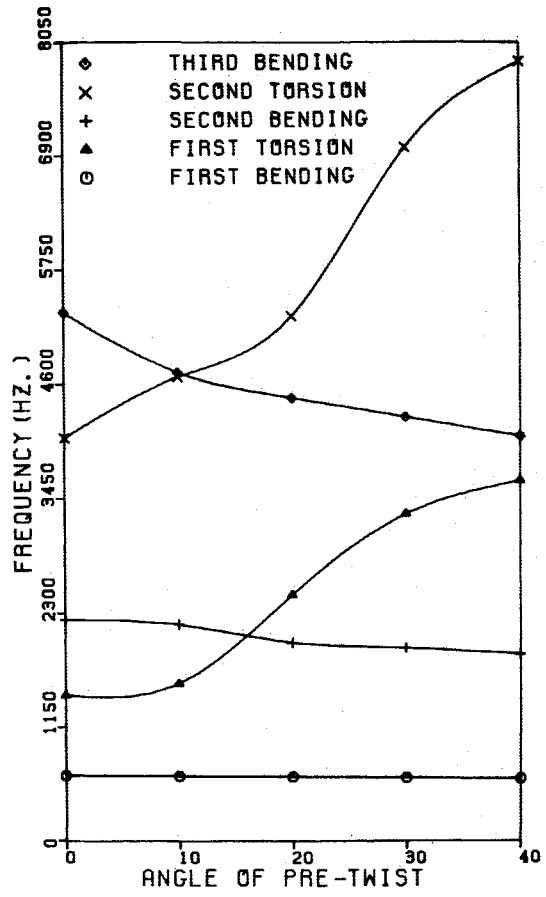

Fig. 7 Variation of natural frequency with pretwist.

Conclusion

In the present work, the free vibration study of the rotor blades was carried out using 20 node, solid finite elements. The transient temperature analysis was carried out by solving a nonlinear system of equations. The studies also included the effect of the variation of the natural frequencies with the change in the pretwist angle. In order to reduce the CPU time, a dynamic coordinate reduction scheme also was used. From this investigation, the following conclusions can be drawn:

1) There is a significant difference in the temperature distribution in the turbine blade with and without radiative boundary conditions.

2) The natural frequencies vary quite significantly during the transient heating period.

3) The variation of the pretwist angle has significant influence on the natural frequencies. The bending natural frequencies decrease with the increase in the angle of pretwist; but the effect is just the opposite on the torsional modes.

4) The dynamic matrix reduction scheme can be very fruitfully used in the case of rotor blades.

Appendix A

The force vector due to radiative heat transfer $\{F_R\}$ can be expressed as

$$\{F_r\} = \int_{S_2} \sigma\epsilon T_\infty^4 [N]^T \, dS - \int_{S_2} \sigma\epsilon [N]^T ([N]\{T\})^4 \, dS$$

For side $i-j$ of the triangular element, the force vector due to radiation can be written as

$$\{F_R^e\} = \frac{\sigma\epsilon L_{ij} T_\infty^4}{2} \begin{bmatrix} 1 \\ 1 \\ 0 \end{bmatrix} - \frac{\sigma\epsilon L_{ij}}{30}$$

$$\times \begin{bmatrix} 5T_i^4 + 4T_i^3 T_j + 3T_i^2 T_j + 2T_i T_j^3 + T_j^4 \\ 5T_j^4 + 4T_j^3 T_i + 3T_j^2 T_i + 2T_j T_j^3 + T_j^4 \\ 0 \end{bmatrix}$$

where L_{ij} is the length of the side i-j of the triangle subjected to radiation.

Appendix B

The interpolation functions for the 20 node isoparametric element can be expressed as

Corner nodes:

$$N_i = \tfrac{1}{8}(1 + \xi\xi_i)(1 + \eta\eta_i)(1 + \zeta\zeta_i)(\xi\xi_i + \eta\eta_i + \zeta\zeta_i - 2)$$

Typical midside node:

$$N_i = \tfrac{1}{4}(1 - \xi^2)(1 + \eta\eta_i)(1 + \zeta\zeta_i)$$

for the case when $\xi_i = 0$, $\eta_i = \pm 1$, and $\zeta_i = \pm 1$. Here, subscript i represents the ith node of the 20 node element.

As stated earlier, the $[B]$ matrix is a product of three matrices $[P]$, $[Q]$, and $[R]$. The expressions for these three matrices are

$$[P]_{6\times 9} = \begin{bmatrix} 1 & 0 & 0 & 0 & 0 & 0 & 0 & 0 & 0 \\ 0 & 0 & 0 & 0 & 1 & 0 & 0 & 0 & 0 \\ 0 & 0 & 0 & 0 & 0 & 0 & 0 & 0 & 1 \\ 0 & 1 & 0 & 1 & 0 & 0 & 0 & 0 & 0 \\ 0 & 0 & 1 & 0 & 0 & 0 & 1 & 0 & 0 \\ 0 & 0 & 0 & 0 & 0 & 1 & 0 & 1 & 0 \end{bmatrix}$$

$$[Q]_{9\times 9} = \begin{bmatrix} J_{11}^{-1} & J_{12}^{-1} & J_{13}^{-1} & 0 & 0 & 0 & 0 & 0 & 0 \\ J_{21}^{-1} & J_{22}^{-1} & J_{23}^{-1} & 0 & 0 & 0 & 0 & 0 & 0 \\ J_{31}^{-1} & J_{32}^{-1} & J_{33}^{-1} & 0 & 0 & 0 & 0 & 0 & 0 \\ 0 & 0 & 0 & J_{11}^{-1} & J_{12}^{-1} & J_{13}^{-1} & 0 & 0 & 0 \\ 0 & 0 & 0 & J_{21}^{-1} & J_{22}^{-1} & J_{23}^{-1} & 0 & 0 & 0 \\ 0 & 0 & 0 & J_{21}^{-1} & J_{22}^{-1} & J_{23}^{-1} & 0 & 0 & 0 \\ 0 & 0 & 0 & 0 & 0 & 0 & J_{11}^{-1} & J_{12}^{-1} & J_{13}^{-1} \\ 0 & 0 & 0 & 0 & 0 & 0 & J_{21}^{-1} & J_{22}^{-1} & J_{23}^{-1} \\ 0 & 0 & 0 & 0 & 0 & 0 & J_{31}^{-1} & J_{32}^{-1} & J_{33}^{-1} \end{bmatrix}$$

$$[R] = \underset{9\times 60}{\begin{bmatrix} \frac{\partial N_1}{\partial \xi} & 0 & 0 & \frac{\partial N_2}{\partial \xi} & 0 & 0 & \frac{\partial N_3}{\partial \xi} & - & - & - & - \\ \frac{\partial N_1}{\partial \eta} & 0 & 0 & \frac{\partial N_2}{\partial \eta} & 0 & 0 & \frac{\partial N_3}{\partial \eta} & - & - & - & - \\ \frac{\partial N_1}{\partial \zeta} & 0 & 0 & \frac{\partial N_2}{\partial \zeta} & 0 & 0 & \frac{\partial N_3}{\partial \zeta} & - & - & - & - \\ 0 & \frac{\partial N_1}{\partial \xi} & 0 & 0 & \frac{\partial N_2}{\partial \xi} & 0 & 0 & - & - & - & - \\ 0 & \frac{\partial N_i}{\partial \eta} & 0 & 0 & \frac{\partial N_2}{\partial \eta} & 0 & 0 & - & - & - & - \\ 0 & \frac{\partial N_1}{\partial \zeta} & 0 & 0 & \frac{\partial N_2}{\partial \zeta} & 0 & 0 & - & - & - & - \\ 0 & 0 & \frac{\partial N_1}{\partial \zeta} & 0 & 0 & \frac{\partial N_2}{\partial \xi} & 0 & - & - & - & - \\ 0 & 0 & \frac{\partial N_1}{\partial \eta} & 0 & 0 & \frac{\partial N_2}{\partial \xi} & 0 & - & - & - & - \\ 0 & 0 & \frac{\partial N_1}{\partial \zeta} & 0 & 0 & \frac{\partial N_2}{\partial \zeta} & 0 & - & - & - & - \end{bmatrix}}$$

The shape function matrix used in the evaluation of the elemental consistent mass matrix $[M^e]$ can be expressed as

$$[N] = \underset{3\times 60}{\begin{bmatrix} N_1 & 0 & 0 & N_2 & 0 & 0 & N_3 & 0 & 0 & - & - & - \\ 0 & N_1 & 0 & 0 & N_2 & 0 & 0 & N_3 & 0 & - & - & - \\ 0 & 0 & N_1 & 0 & 0 & N_2 & 0 & 0 & N_3 & - & - & - \end{bmatrix}}$$

Acknowledgments

The authors are thankful to the Natural Science and Engineering Council of Canada for their Grant A5549, which was used as a financial support for this work.

References

[1]Subrahmanyam, K. B. and Leissa, A. W., "An Improved Finite Difference Analysis of Uncoupled Vibrations of Cantilever Beams," *Journal of Sound and Vibration,* Vol. 98, Jan. 1985, pp. 1–11.

[2]Hutchinson, J. R. and Zillmer, S. D., "On the Transverse Vibration of Beams of Rectangular Cross-Section," *Journal of Applied Mechanics,* Vol. 53, No. 1, March 1986, pp. 39–44.

[3]Banerji, J. R. and Williams, F. W., "Exact Bernoulli-Euler Dynamic Stiffness Matrix for a Range of Tapered Beams," *International Journal of Numerical Methods in Engineering,* Vol. 21, Dec. 1985, pp. 2289–2302.

[4]Gupta, A. K., "Vibration of Tapered Beams," *Journal of Structural Engineering* (ASCE), Vol. 111, Jan. 1985, pp. 19–31.

[5]Sisto, F. and Chang, A. T., "A Finite Element for Vibration Analysis of Twisted Blades Based on Beam Theory," *AIAA Journal,* Vol. 22, Nov. 1984, pp. 1646–1651.

[6]Reddy, B. S. and Sharan, A. M., "The Transient Heat Transfer Analysis of Solids with Radiative Boundary Condition Using Finite Element Analysis," *International Communications on Heat and Mass Transfer,* Vol. 12, 1985, pp. 169–178.

[7]Allen, J. M., "Effect of Temperature Dependent Mechanical Properties on Thermal Stresses in Cooled Turbine Blades," *Transactions of ASME, Journal of Engineering for Power,* Vol. 104, April 1982, pp. 349–353.

[8]Mukherjee, D. K., "Stresses in Turbine Blades Due to Temperature and Load Variation," American Society of Mechanical Engineers, New York, ASME Paper 78-GT-158, 1978.

[9]Maya, T., Katsumata, I., and Itoh, M., "A Study of Thermal Fatigue Life Prediction of Air-Cooled Turbine Blades," American Society of Mechanical Engineers, New York, ASME Paper 78-GT-63, 1978.

[10]Zienkiewicz, O. C., *The Finite Element Method,* McGraw-Hill, London, 1977, pp. 169–171.

[11]Huebner, K. H. and Thornton, A. E., *The Finite Element Method for Engineers,* Wiley, New York, 1982, pp. 187, 513–518.

[12]Guyan, R. J., "Reduction of Stiffness and Mass Matrices," *AIAA Journal,* Vol. 3, Feb. 1965, p. 380.

[13]Cubberly, W. H., *ASM Metals Reference Book,* Vol. 3, 9th ed., American Society for Metals, Metals Park, OH, 1980, pp. 248–249.

[14]Rao, J. S. and Vyas, N. S., "Response of Steam Turbine Blades Subjected to Distributed Harmonic Nozzle Excitation," 3rd International Modal Analysis Conference, Orlando, FL, 1985.